Montoya, A., Rodríguez-Sánchez, M., López-Puente, J. & Santana, D. (2018). Numerical model of solar external receiver tubes: Influence of mechanical boundary conditions and temperature variation in thermoelastic stresses. *Solar Energy, 174*, 912–922.

DOI: 10.1016/j.solener.2018.09.068

Numerical model of solar external receiver tubes: influence of mechanical boundary conditions and temperature variation in thermoelastic stresses

Andrés Montoya[a,*], M.R. Rodríguez-Sánchez[b], Jorge López-Puente[a], Domingo Santana[b]

[a] *Continuum Mechanics and Structural Analysis Department, Universidad Carlos III de Madrid, Avda. de la Universidad, 30, 28911 Leganés, Madrid, Spain*
[b] *Department of Thermal and Fluid Engineering, Universidad Carlos III de Madrid, Avda. de la Universidad, 30, 28911 Leganés, Madrid, Spain*

Abstract

Failure in solar external receivers is mainly originated from the thermal stress, caused by the high non-uniform transient solar flux. The heat-up and cooldown of tube receivers in daily cycles produces low-cycle fatigue that limit the lifetime of tubes. The corrosion of tube materials produced by incompatibility between the decomposed heat transfer fluid and tube material may increase this issue.

The temperature spatial distribution in these tubes has strong variations in radial, circumferential, and axial directions. The stress field, produced by the temperature gradients, has been commonly analyzed using bidimensional models in isolated tube cross sections, without taking into account the axial temperature variation, the mechanical boundary conditions, and the temperature-dependent thermomechanical properties.

*Corresponding author. Tel +34 916248809
Email address: andmonto@ing.uc3m.es (Andrés Montoya)

October 10, 2018

In this work a three dimensional finite element model has been developed in order to calculate the stress field distribution, without performing any geometrical simplification. In addition, appropriate mechanical boundary conditions have been imposed in order to adequately simulate the tube behavior. Besides, radial, circumferential and axial temperature variations have been studied separately to analyze how each of them influences the maximum stress distribution. This 3D model has been compared with analytical solutions for the two-dimensional thermal stress problem in circular hollow cylinders.

The results show that the boundary conditions have a significant effect in the tube stresses, increasing the axial stress component and therefore the equivalent stress.

The analysis of each of the temperature variations showed that the circumferential variation temperature is the one that produces most of the stress, since it tries to strongly bend the tube, which is impeded by the boundary conditions.

The results also present that 2D models are not capable of obtaining the correct stress distribution along the tube, since they are supposing that the temperature does not vary axially. By contrast, the maximum stress can be obtained with confidence using the analytical stress solution of the angular and radial temperature variation around a hollow circular cylinder.
Keywords: Solar external receiver; Thermal stress; Temperature gradients; Thin-walled cylinder

---

1. Introduction

Molten salt external receivers are tubular heat exchangers subjected to complex thermo-mechanical loads. The cyclic and non-homogeneous heat flux distribution is responsible for temperature gradients and thermal stresses, and the boundary conditions of the tubes caused by the supports increase these stresses. The most important role of solar central receivers is to keep the intercept solar flux within the tube mechanical safety limits.

Thermal stresses are produced when a temperature variation of the material occurs in presence of constraints (Barron and Barron, 2011). Solids present internal constraints that originate thermal stresses; they appear because strong temperature gradients promotes different dilatation displacements for vicinity material points.

Thermal stresses could be produced also by external constraints, like supports. These constraints prevent some displacements of the system in presence of temperature gradients. Reaction forces appear in the supports to prevent the displacement of the system, which must be limited to avoid shades and contact between tubes, since it may cause overcooling and overheating respectively.

Nowadays, the direct measurement of the incident solar flux distribution, the tube wall temperature and the stress profiles is impracticable during the receiver operation. An inaccurate estimation of the tube wall temperature and the stresses can damage the tubes, risking the whole power plant operation. Therefore, the development of thermo-mechanical models to predict the temperature and the stresses in the tubes of the receiver is of great interest.

Numerous are the thermal and mechanical models that can be found in

the literature to analyze solar receivers. However, most of them are only focus in the thermoelastic behavior of these systems, forgetting the mechanical restrictions: Kent and Ark (1931) analyzed thermal stress in thin-walled cylinders, with temperature variation in radial and axial directions, however, not in the circumferential one. Goodier (1937, 1957), studied the thermal stress in thin-walled cylinders whose thickness and temperature distribution may vary around the circumference. Sauer (1996) developed formulae for the analysis of axial stress in pipes due to thermal stratification, but with no radial temperature variation. Wagner (2008) developed a complete model to analyze the receivers behavior, however he considered no circumferential variation on the wall temperature of the tubes. Du et al. (2016) developed a model to analyze the thermal stresses and the fatigue in molten salt receivers using basic thermal elasticity equations and they compared it with numerical simulations; they considered circumferential variation of the incident solar flux, but they did not take into account the mechanical restrictions of the tubes. Neises et al. (2014) developed an approach to calculate the thermal and pressure stresses on the receivers, without considering mechanical constraints. Marugán-Cruz et al. (2016) carried out a numerical study of the stresses in thin-walled pipes subjected to a non-uniform heat flux using Gatewood (1941) formulation. They highlighted the importance of the Reynolds, Prandtl and Biot numbers in the problem; however, they did not consider the external constraints. Irfan and Chapman (2009) characterized the thermal stresses in radiant tubes due to axial, circumferential and radial temperature gradients; although these tubes were not part of a solar receiver, they showed very interesting results, even if they assumed no

mechanical restrictions in the tubes. Recently, Logie et al. (2018) calculated the 2D thermoelastic stress in concentrating solar receiver tubes employing classical thermoelasticity equations.

There are other studies related to the stress in solar receivers that are not focus on the tube characterization. For example, Wang et al. (2012) studied how to select the most adequate material in the receiver as a function of the thermal stresses; they pointed that stainless steel has a high failure ratio, however, it is the most typical material in the receivers. Uhlig et al. (2017) considered the mechanical restrictions of the receiver, focusing their analysis in the stresses that occur in the panel headers due to the ovens heating.

This study is focused on the characterization of the thermal stresses produced by the two types of constraints, internal and external, in molten salt solar receivers. The stress origin will be studied in order to understand how these constraints affect the stress distribution. Besides, the importance of internal and external constraints has been studied separately considering or not the supports along the tubes.

This work is organized as follows: in the following section the receiver geometry and constraints have been defined. In section 3 the models used to characterize the thermal and mechanical behavior of the receiver have been described. In section 4 the methodology developed by Logie et al. (2018) to calculate thermal stress is introduced. Section 5 shows the results obtained with the numerical model, for different boundary conditions. Besides, numerical and analytical results are compared in section 5. Finally, the main conclusions of this study are presented in section 6.

2. Studied geometry

To calculate the thermal stresses in a receiver tube, a solar power tower with molten salt as heat transfer fluid, similar to Gemasolar, has been analyzed.

Gemasolar solar plant is located in Fuentes de Andalucía, Spain, at 37.56° north latitude. Its solar field is radial staggered layout slightly biased to the north, with the highest radius equal to 850 m. Gemasolar field consists of 2650 square heliostats of 10.95 m side, which are distributed in three different zones: the inner one has a radial cornfield configuration and the two external zones are staggered. The position of each heliostat has been determined with scaled aerial images of the solar plant. The reflectivity, the cleanliness and the tracking errors of the mirrors have been obtained from Sánchez-González et al. (2017).

Gemasolar receiver tower is 120 m high. The solar receiver is a cylindrical absorber with 10 m height and an aspect ratio of 1.17. The circular perimeter is composed by 18 vertical panels of 1.5 meters width, integrated each of them by 60 tubes of 2.24 cm external diameter and 1.2 mm thickness. Stainless steel with high nickel content is the preferable material in solar receivers; since no information of the tube material has been obtained, alloy 800H has been selected as the tube material. To increase the tubes absorptivity, they are coated on the outside face with black Pyromark.

The receiver tubes intercept the solar radiation reflected by the heliostats and transmit it to the heat transfer fluid (HTF) that flows inside them. In Gemasolar, the HTF is solar salt (60% $NaNO_3$ - 40% KNO_3) that enters in the receiver at 290 °C and exits at 565 °C. The mass flow rate of molten salt

in the receiver depends on the incident solar flux. For the case studied in this work, the total mass flow rate in the receiver is 257.7 kg/s which corresponds to the solar noon of the Spring Equinox.

Tubes are joined to an inlet and an outlet header in all the panels. The header located at the top of the receiver is attached to the receiver support frame. The receiver panel support frame is a close tolerance structural element that supports and guides the tube header assembly at the top, allowing free expansion of the tubes and bottom header (in the downward direction). The tubes in the panels are separated between them only 2.5 mm (Litwin, 2002), thus to avoid overheating of the tubes by contact, the frame restrains the tubes from bowing outwards and laterally, and also prevents the appearance of gaps between the tubes and the backside of the receiver. To achieve that, each tube is periodically guided over their entire length by clips (McDowell and Miner, 2013), see Fig. 1. These clips are individually welded to each tube. The attachment of the tube clips to the tubes it is designed and tested to assure that the applied weld procedure limits the penetration to the tube wall to the minimum amount necessary to assure complete fusion. Full penetration, pinholes, and burn-through are not permitted (Zavoico, 2001).

In order to take into account the mechanical boundary conditions previously mentioned, the upper part of the tubes has been considered encastred, and the opposite end of the tube can displace freely. Besides, the tube clips have been assumed as mobile supports that only allow 1 degree of freedom in the movement (axial direction); the distance between clips is 2 m. All the boundary conditions and the geometry of the tube are shown in Fig. 2.

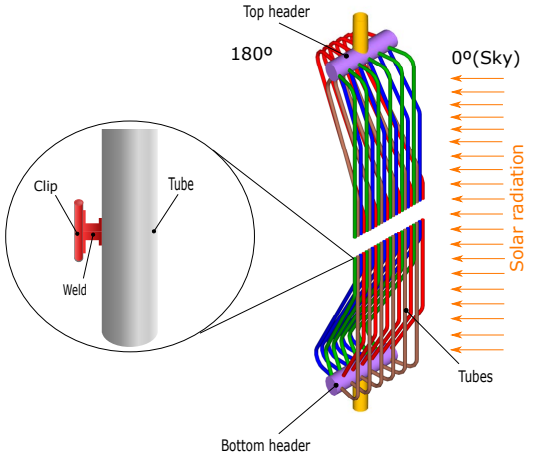

Fig. 1: Schematic of a receiver panel and detail of the clips.

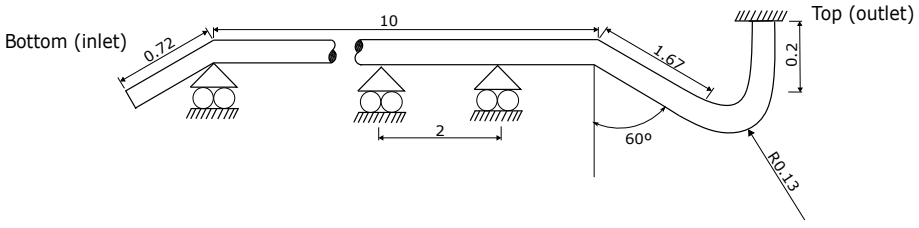

Fig. 2: Tube geometry used in the thermoeslastic model, measurement in meters. It is rotated 90° from its original vertical position

3. Methodology

3.1. Optical and thermal model

The optical model FluxSPT[1] developed by Sánchez-González and Santana (2015) has been used to calculate the incident solar flux distribution on the receiver. The concentration ratio is calculated with a projection method, and the flux distribution is based on a circular Gaussian resulting from the convolution of the sunshape and the heliostat slope. This model has low

[1] `ise.uc3m.es/research/solar-energy/fluxspt`

computational cost and can be adapted to different solar fields and receiver geometries. Besides, it allows modifying the aiming strategy. In this case, it has been assumed that all the heliostats aim to the center of the receiver (equatorial aiming).

Once the incident solar flux on the receiver is known, the thermal model developed by Rodríguez-Sánchez et al. (2014) has been used to characterize the heat exchange and the temperature profile in the tubes of the receiver. This model obtains the temperature profiles in the inner and outer wall of the tubes and in the molten salt solving the radiative and convective heat transfer in the tubes of the receiver, the tube conduction in the tube walls, and the internal convection of the HTF (see Fig. 3).

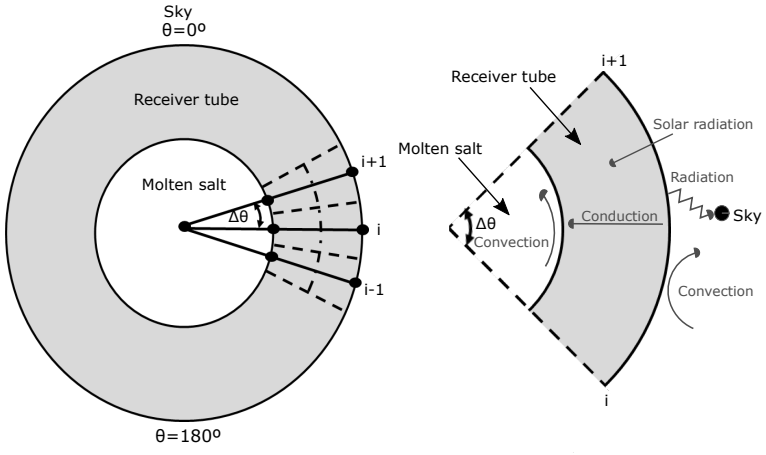

Fig. 3: Optical-thermal conversion process in a receiver tube.

To reduce the computational cost, the thermal model only solves one representative tube per panel, assuming that in each panel all the tubes have the same behavior. However, it takes into account the heat exchange between adjacent tubes and the surroundings. One of the main characteristic

of this model is that considers circumferential and axial variations of the incident heat flux and the wall temperature, which will be essential for the characterization of the stresses that appear in the receiver tubes.

For the calculations, the tubes have been divided in 39 vertical segments, and 72 circumferential sections. This model also takes into account the properties variation with the temperature of the HTF (Zavoico, 2001) and the tube material (American Society of Mechanical Engineers, 2010). Typical ambient conditions of Seville (where Gemasolar is located) have been considered to carry out the simulations.

This model also takes into account the properties variation with the temperature of the HTF (Zavoico, 2001) and the tube material (American Society of Mechanical Engineers, 2010). Typical ambient conditions of Seville (where Gemasolar is located) have been considered to carry out the simulations.

3.2. Thermoelastic model with solid and shell elements

Although the thermal model solves the whole receiver, for the thermoelastic model only the first panel of the receiver has been analyzed, because it receives the highest solar flux intensity. Therefore, the tubes of this panel have the highest temperature gradient, that implies higher thermal stresses and deformations.

Temperature distribution (inner and outer tube wall temperature) of this first panel is exported to a thermoelastic model, developed in the finite element program Abaqus/Standard, as a boundary condition. The thermoelastic model computes the temperature through the tube thickness and the resultant stresses and deformations. A coupled thermal-displacement analysis has been used in stationary state.

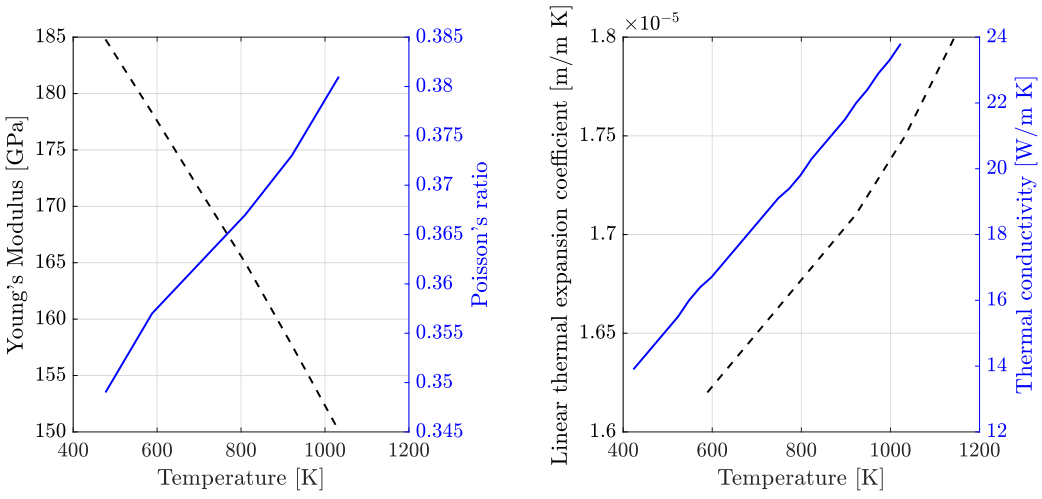

(a) (b)

Fig. 4: Temperature-dependent properties of 800H alloy (American Society of Mechanical Engineers, 2010) used in the simulation (a) Young's modulus and Poisson's ratio, (b) linear thermal expansion coefficient and thermal conductivity.

Tube material has been studied in a linear elastic regime, because tubes do not suffer plastic deformation in the present working conditions. Fig. 4 depicts the temperature-dependent material properties taken from the American Society of Mechanical Engineers (2010).

In order to obtain the 3D stress tensor, solid elements should be used. Since at least five elements have to be placed along the thickness, keeping the aspect ratio of the element in circumferential and axial directions would lead to a prohibitive number of elements ($\sim 10^7$). Since the thickness is much smaller than the radius, shell elements are recommended, however, shell elements do not provide the complete stress tensor.

To overcome this issue, an intermediate solution can be adopted. The tube has been modelled using shell elements but one "slice" of 12 mm thick

(10 times the tube thickness) has been discretized using solid elements, placed where the highest temperature value is located. Shell-to-solid coupling interaction has been used in order to couple the displacement of the shell edge to the adjacent solid face. Therefore, stresses can be analyzed in the solid slice taking into account the complete stress tensor.

There are thirty-six 4-node linear shell elements (with five integration points through the thickness) in the circumferential direction, and five thousand in the axial direction (element size 2 mm). On the other hand, the solid slice has been discretized in order to have five 20-node quadratic elements in its radial direction, so the number of integration points along the thickness is doubled in the solid slice compared to the shell part. This condition creates solid elements of 0.24 mm size. The total number of elements used is 276240 (231840 shell elements and 44400 solid elements). If all the tube were discretized with solid elements, it would have 3.7 million elements per meter.

4. Analytical approach to thermal stresses calculation

A method presented by Logie et al. (2018), which uses the approximation of two-dimensional thermoelasticity from Timoshenko and Goodier (1951), Boley and Weiner (1997) and Hetnarski and Eslami (2010), has been used to calculate analytically the stresses in hollow cylinders and to compare the results with the three dimensional model proposed in the present work.

To use the analytical solution, the inner and outer wall temperature distributions of the tubes have to be described using Fourier series as follows:

$$T_i = \overline{T}_i + \sum_{n=1}^{\infty} B'_n \cos n\Theta + D'_n \sin n\Theta \tag{1}$$

$$T_o = \overline{T}_o + \sum_{n=1}^{\infty} B''_n \cos n\Theta + D''_n \sin n\Theta \tag{2}$$

Only terms of $n = 0$ and $n = 1$ are the only ones that produce stress, since the net heat flow corresponding to terms $\cos 2\Theta$, $\sin 2\Theta$ and higher harmonics is zero (Timoshenko and Goodier, 1951). The expressions for average geometrical surface temperatures are:

$$\overline{T}_i = \frac{1}{2\pi} \int_0^{2\pi} T_i d\Theta \tag{3}$$

$$\overline{T}_o = \frac{1}{2\pi} \int_0^{2\pi} T_o d\Theta \tag{4}$$

The circumferentially varying temperature for every point of the tube cross section is defined as:

$$T_\Theta = T(r, \Theta) - (\overline{T}_i - \overline{T}_o) \frac{\ln \frac{b}{r}}{\ln \frac{b}{a}} - \overline{T}_o \tag{5}$$

The stress equations for non-axisymmetrical heating are:

$$\sigma_r = K \frac{\alpha E}{2(1-\nu)} \left[-\ln \frac{b}{r} - \frac{a^2}{b^2 - a^2} \left(1 - \frac{b^2}{r^2} \right) \ln \frac{b}{a} \right] + K_\Theta \frac{\alpha E}{2(1-\nu)} \left(1 - \frac{a^2}{r^2} \right) \left(1 - \frac{b^2}{r^2} \right) \tag{6}$$

$$\sigma_\Theta = K \frac{\alpha E}{2(1-\nu)} \left[-\ln \frac{b}{r} - \frac{a^2}{b^2 - a^2} \left(1 - \frac{b^2}{r^2} \right) \ln \frac{b}{a} \right] + K_\Theta \frac{\alpha E}{2(1-\nu)} \left(3 - \frac{a^2 + b^2}{r^2} - \frac{a^2 b^2}{r^4} \right) \tag{7}$$

where the K term is related to the mean radial temperature variation as

follows:

$$K = \frac{\overline{T}_i - \overline{T}_o}{\ln \frac{b}{a}} \tag{8}$$

The contribution of the circumferential temperature variation, comes from K_Θ, which in terms of the Fourier series coeffcients from Eqs 1 and 2 corresponds to:

$$K_\Theta = \frac{rab}{b^2 - a^2}\left[\left(\frac{B_1' b - B_1'' a}{a^2 + b^2}\right)\cos\Theta + \left(\frac{D_1' b - D_1'' a}{a^2 + b^2}\right)\sin\Theta\right] \tag{9}$$

If the assumption of zero axial force is given, the integration of axial stress σ_z over the tube cross section is equal to zero ($\int_A \sigma_z \mathrm{d}A = 0$), and when external mechanical loads are also zero, the axial stress is given by the generalised plane strain equation ($\varepsilon_z = \text{constant}$):

$$\sigma_z = \nu(\sigma_r + \sigma_\Theta) + \alpha E(\overline{T} - T) \tag{10}$$

The axial stress can be calculated substituting Eqs. 6 and 7 in Eq. 10:

$$\sigma_z = K\frac{\alpha E}{2(1-\nu)}\left[1 - 2\ln\frac{b}{r} - \frac{2a^2}{b^2 - a^2}\ln\frac{b}{a}\right] + K_\Theta \frac{\alpha E}{1-\nu}\left(2 - \frac{a^2 + b^2}{r^2}\right) - \alpha E T_\Theta \tag{11}$$

Eq. 11 is valid for a cylinder that is not able to displace perpendicularly to the axial direction (infinite clips along its length).

5. Results and discussion

For an equatorial aiming strategy, the outer and inner wall temperature distribution of the tubes located at the first panel of the receiver has been

obtained from the optical and thermal model. The outer temperature distribution is shown in Fig. 5. The tube surface facing the heliostats has the coordinate $\Theta = 0°$, which corresponds to the highest incident flux, and then to the maximum circumferential temperature. The highest wall temperature is located in $\Theta = 0°$ and $z = 5.5$ m. Stress, solved in the thermoelastic model, depends entirely on these thermal conditions.

The maximum temperature is not located at the center of the tube because the projection of the heat flux from the heliostats in the receiver plane causes an slight vertical deviation of the resultant flux map (Sánchez-González and Santana, 2015). Besides the ascending flow of the HTF also contributes to the upwards displacement of the maximum temperature peak.

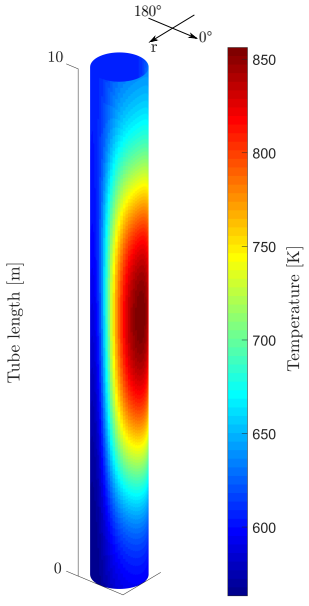

Fig. 5: Temperature profile in the outer tube wall obtained with the optical and thermal model. The diameter is magnified for more clarity.

The main goal of this analysis is to know the stress distribution in molten salt receivers, and the relevance of the internal and external constraints on the thermal stress. To carry out the analysis, two different mechanical boundary conditions have been considered. Firstly, tube receiver has been studied without supports along its length (without clips), with only the upper part of the tube encastred, so the tube can displace freely and only thermal stresses due to internal contraints because of temperature gradients appear. The tube has also been studied considering the clips along its length, so the reactions forces caused by the supports preventing the deflection are present in this second case.

The thermal stresses, studied in the solid section of the model without clips, are shown in Fig. 6. It can be observed that the highest stress components are the axial stress σ_z (250 MPa, see Fig. 6c) and the circumferential stress σ_Θ (-110 MPa, see 6b). Radial stress (σ_r) and shear stress components differ by one order of magnitude from σ_z.

The temperature gradient in radial direction, whose highest value is located at $\Theta = 0°$ and $z = 5.5$ m, does not allow the free expansion of the outer wall, compressing it in axial direction (σ_z) since inner and outer wall are not free to displace independently. The circumferential variation of the temperature produces the tube bending (Barron and Barron, 2011), being this circumferential variation the reason of the high tensile stress in the lateral part of the section ($\Theta = 90°, \Theta = 270°$).

The stresses showed before would produce the tube displacement shown in Fig. 7a. It can be seen that the bottom part of the tube suffers a displacement perpendicular to the axial direction of 7 m. Of course this displacement is

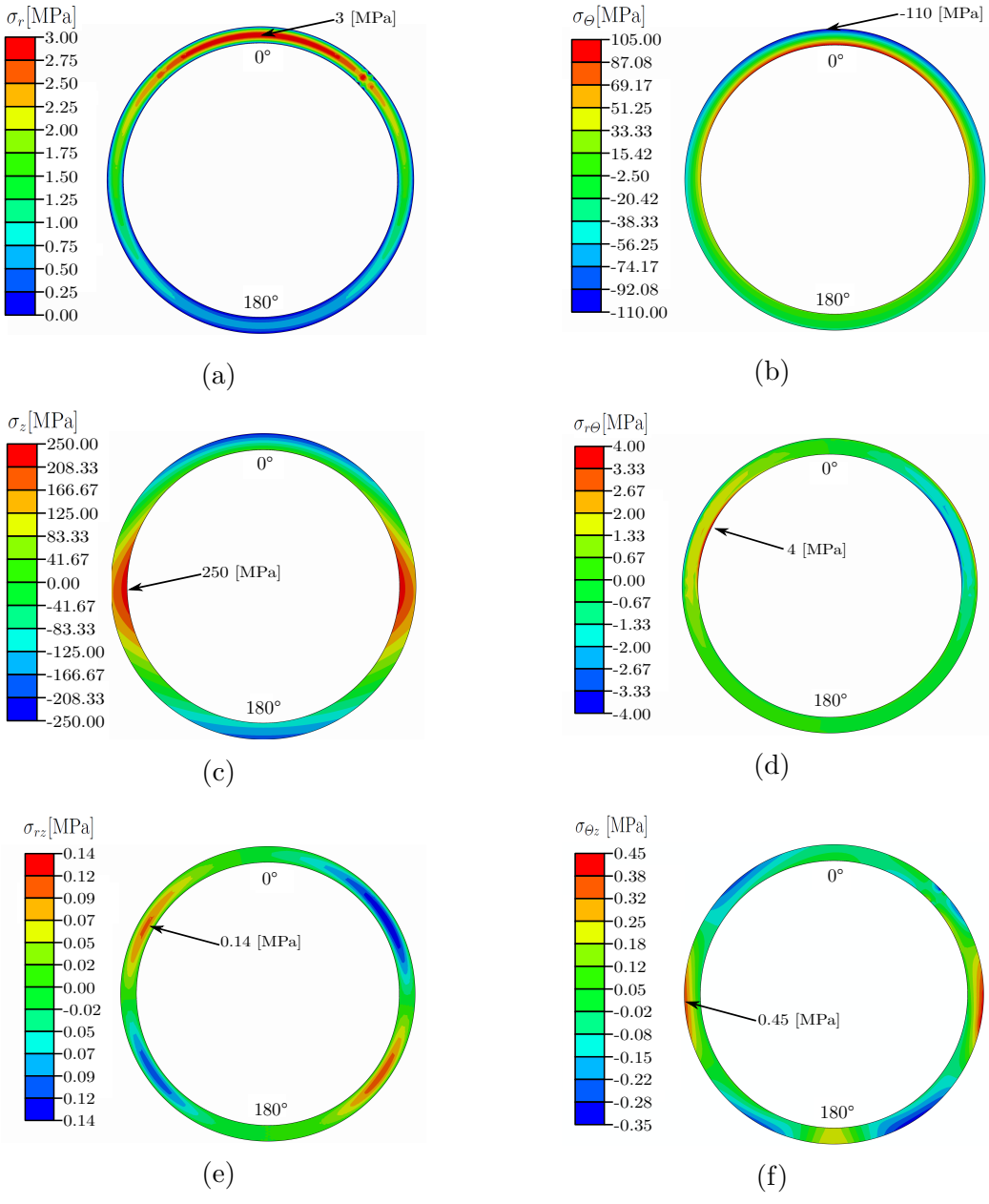

Fig. 6: Normal stress components [MPa] a)σ_r, b)σ_Θ, c)σ_z and shear stress components [MPa] d)$\sigma_{r\Theta}$, e)σ_{rz}, f)$\sigma_{\Theta z}$ in solid slice, for the tube without clips.

prevented in the receiver using clips. Fig. 7b depicts the displacement when the clips are attached to the tube; in this case the maximum displacement found is 2.54 mm. Displacement is limited in the tube with clips, so reaction forces in the constrained points appears, and therefore the stresses.

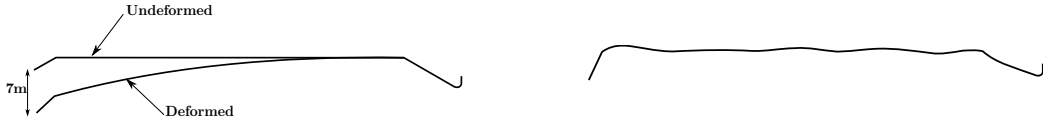

(a) (b)

Fig. 7: Deformation of the tube (a) without clips (scale factor 1/6 compared with undeformed shape) (b) with clips (scale factor 250/1 compared with undeformed shape).

When tube stress is studied with clips, the only substantial change from the previous case occurs in the axial stress component σ_z, as Fig. 8 depicts. Thermal stress only increases in the axial direction due to the influence of reactions in the supported points of the tube (external constraints), so the other stress components remains the same. The reaction force in the clips compress the front part of the tube (already compressed), so the total stress value will be the sum of the thermal stress caused by the internal and external constraints, which takes a value of 660 MPa.

In order to understand the influence of the clips on the stress, equivalent stress (Von Mises) for tubes with and without clips are shown in Fig. 9. Von Mises equivalent stress expression is the following:

$$\sigma_{VM} = \sqrt{{\sigma_r}^2 + {\sigma_\Theta}^2 + {\sigma_z}^2 - (\sigma_r\sigma_\Theta + \sigma_\Theta\sigma_z + \sigma_r\sigma_z) + 3({\sigma_{r\Theta}}^2 + \sigma_{\Theta z}^2 + \sigma_{rz}^2)} \tag{12}$$

Equivalent stress for the clips case is 583 MPa with its maximum value

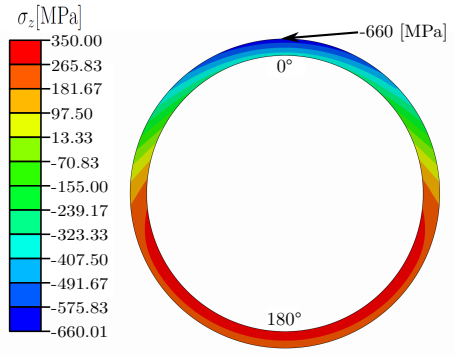

Fig. 8: Axial stress component, σ_z [MPa] in the tube with clips

located at the side of the cross section exposed to the heliostats ($\Theta = 0°$). For the case without clips, equivalent maximum stress is 225 MPa, around two times and a half lower, and is located at the lateral part of the cross section ($\Theta = 90°, \Theta = 270°$). In Fig. 9b, the peak stress facing the heliostats is consistent with how tubes fail, since primarly cracking occurs perpendicular to maximum principal stress direction which, in this case, is the axial direction.

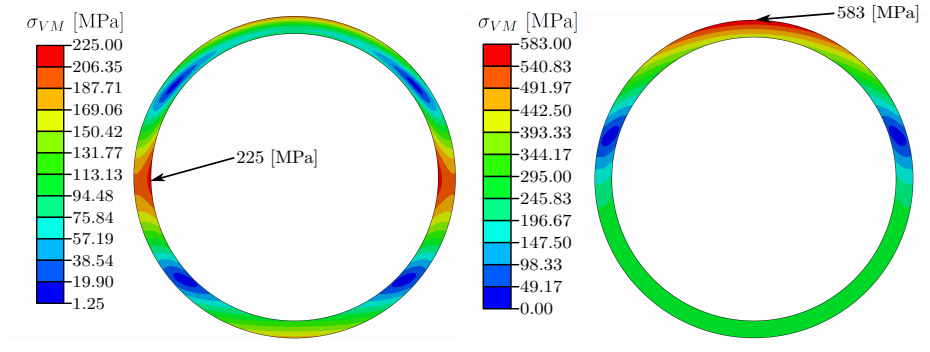

Fig. 9: Von Mises stress [MPa] in solid slice (a) without clips (b) with clips.

Stress in solid and shell regions have been also compared. Fig. 10a

depicts the equivalent stress in the shell-to-solid area. Fig. 10b.b shows the equivalent stress at the same point for the tube discretized only with shell elements. The difference between shell and solid equivalent stress values are about 4%. This difference appears probably because shell elements does not take into account some stresses tensor components.

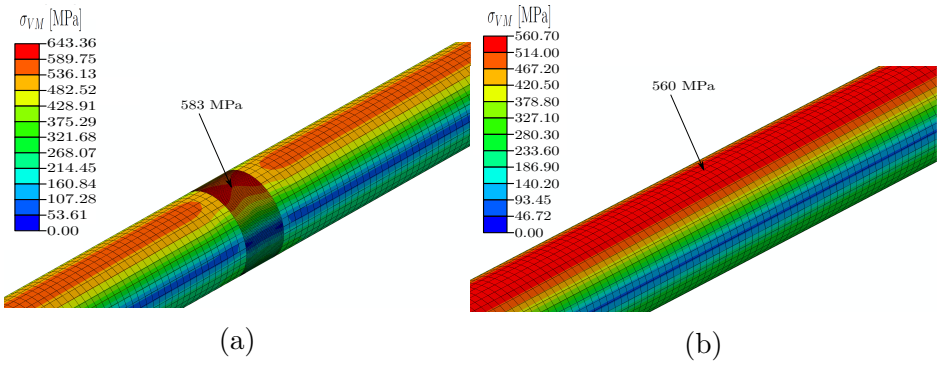

Fig. 10: Von Mises stress [MPa] in outer tube wall, (a) in solid element and (b) in shell elements, for the same point ($z = 5.5$ m)

As the results show, shell elements can be used instead of solid elements for the analyzed problem, because shell elements take into account axial and circumferential stress components, which are the most important ones, therefore the error made is small. The computational cost of using shell elements is also lower compared with solid elements.

In order to analyze the stress distribution along the tube length, Fig. 11 depicts the outer wall temperature and the equivalent stress at $\Theta = 0°$. It can be observed that the temperature (Fig. 11a) and the stress for the case without clips (dashed line in Fig. 11b) has a similar trend. Therefore, with no external constraints, stress depends fully on the temperature along axial direction. The higher is the temperature value the greater will be the stress.

Using clips, the stress distribution (solid line in Fig. 11b) is also similar to the shape of the temperature, but the stress slope varies every 2 m, which coincides with the clips distribution along the tube.

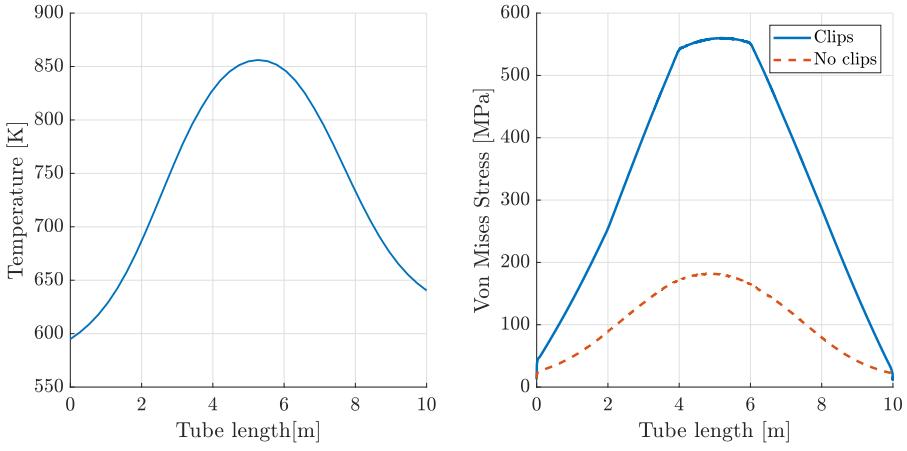

Fig. 11: In $\Theta = 0°$, (a) outer wall temperature [K] and (b) Von Mises stress [MPa] for the case with and without clips.

5.1. Analytical and finite element model comparison

The methodology proposed by Logie et al. (2018) has been used to calculate analytically the thermal stresses in the tube, using Eqs. 6 and 7 for the radial and circumferential stresses respectively, independly of the mechanical boundary conditions. The stress in the axial direction z has been calculated with Eq. 11.

Using a curve fitting tool, coefficients of Eqs. 1 and 2 have been obtained from the inner and outer temperature distributions calculated with the thermal model. The thermal expansion coefficient (Fig. 4b) used is the corresponding to the maximum cross section temperature. Coefficients obtained to characterize the temperature distribution are summarized in Table 1. Note that since the temperature distribution is almost symmetrical about $\Theta = 0° - 180°$ axis, the contribution of sinusoidals terms are negligible.

Coefficient	Value [K]
$\overline{T}_i$	661.7
$\overline{T}_o$	683.6
B_1'	-109.3
B_1''	-139.2
D_1'	0.03648
D_1''	1.924e-8

Table 1: Estimated coefficients for Eqs. 1 and 2.

The temperature distribution fitted corresponds to $z = 5.5$ m, where the outer temperature is maximum. After determinating coefficients K (Eq. 8), K_Θ (Eq. 9), and the circumferentially varying temperature values T_Θ (Eq. 5), stresses can be calculated. The results of the calculated stresses are presented in Figs. 12.

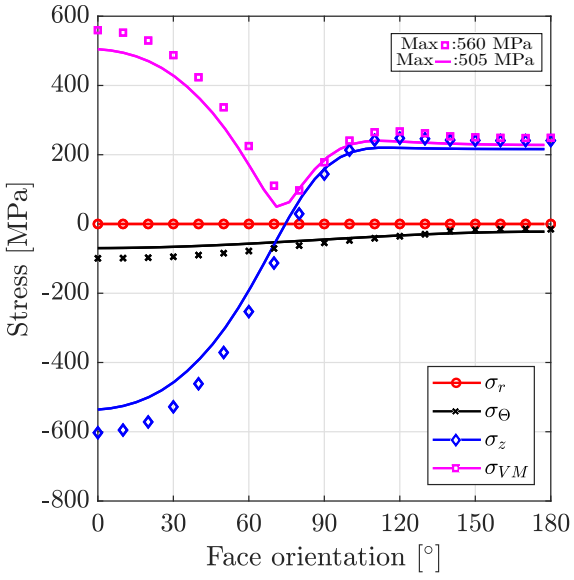

Fig. 12: Stress at the outer tube wall, corresponding to the temperature distribution $z = 5.5$ m when the tube is clips attached. Solid lines indicate results of Eqs. 6, 7 and 11, and markers indicate the results of the numerical model.

As Fig. 12 depicts, stress values from analytical equations and the finite element model are quite similar. In both cases the maximum stress is located at $\Theta = 0°$, where the tube is compressed. The discrepancy between analytical and numerical results may be produced because Eq. 11 does not take into account the fact that the thermal expansion coefficient α, and the other properties are temperature-dependant variables, so the relative displacement between points with different temperature should be higher.

5.2. Temperature influence on stress and deformation

The temperature field in the tube is highly variable, since it varies circumferentially, radially and axially. To better understand the origin of the thermal stresses and deformations, the influence of each of these variations

should be individually studied.

Starting from the actual temperature field obtained with the optical and thermal model, simplified temperature distributions that do not vary in one of the coordinates r,Θ, or z have been analyzed to obtain a simplified stress aproximation. The different temperature profiles and their corresponding stress distributions are shown in Fig. 13. In this section the numerical model has only shell elements.

5.2.1. Temperature field influence without circumferential variation.

To obtain an stress estimation, simplifications are done in the temperature distribution. The first simplification is disaggregated circumferential temperature variation, so axisymmetric temperature distribution $T(r, z)$, has been introduced. The temperature does not vary circumferentially, but radially and axially, as Fig. 13a shows. The selected temperature difference is the highest gradient between the inner and outer wall in the entire tube length: $\Theta = 0°$, $z = 5.5$ m.

Using this temperature distribution, the outer wall, which has a higher temperature than the inner wall, tries to expand more, but the inner wall (colder) constraints the free motion, since they are not free to move independently. This is the reason why outer surface is compressed and inner is under tension (Fig. 13b).

The axisymmetric gradient means that the tube does not bend due to this temperature gradient, therefore external constrains do not induce thermal stress, and its value remains the same with and without clips, as the results from Tables 2 and 3 show.

Radial temperature gradient produces stress in circumferential direction

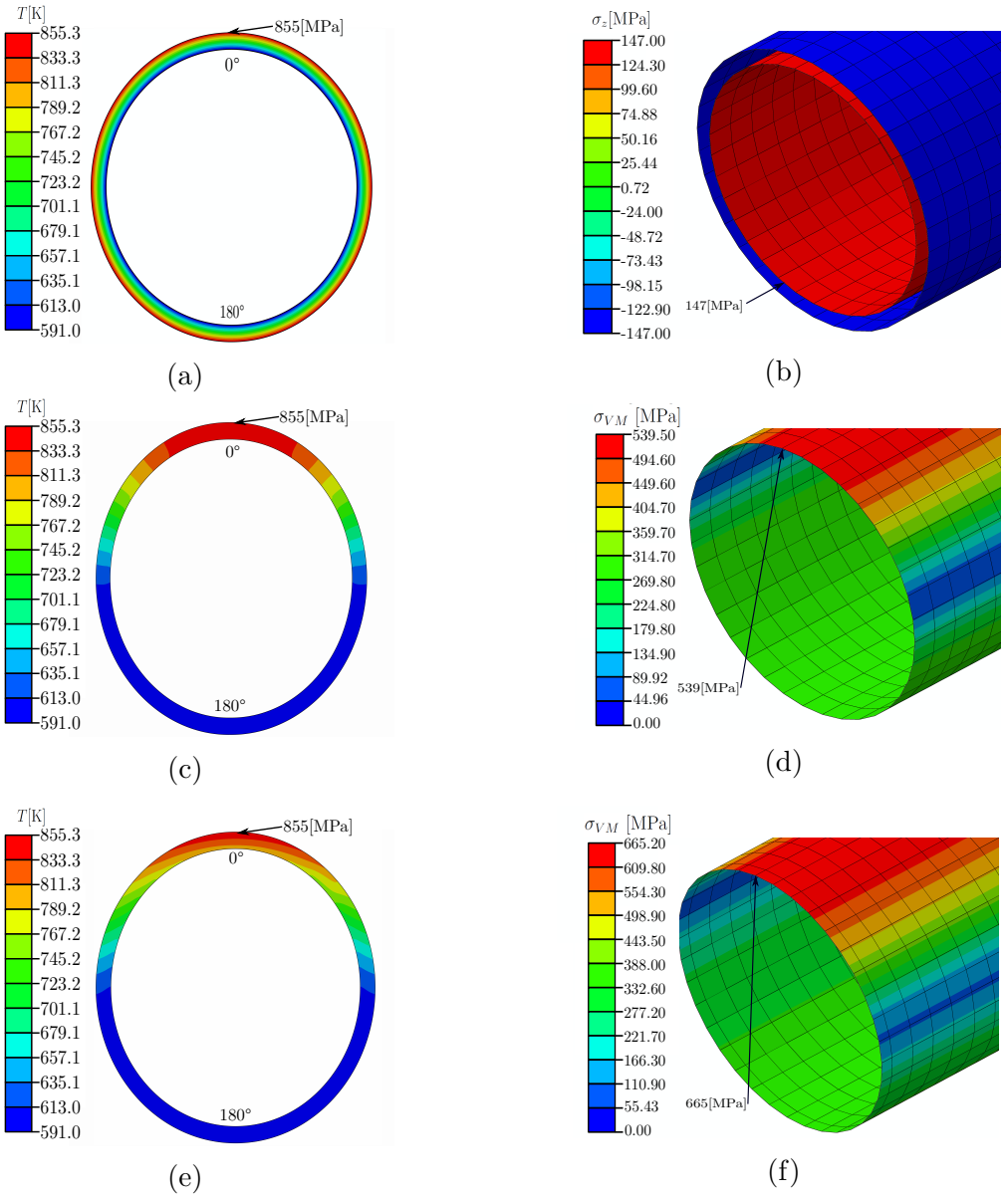

Fig. 13: Temperature gradient [K] in the cross section corresponding to z=5.5 m for temperature distribution (a) $T(r, z)$, (c) $T(\Theta, z)$ (e) $T(r, \Theta)$. Axial stress [MPa] in inner and outer tube walls for (b) $T(r, z)$ and maximum equivalent stress [MPa] for (d) $T(\Theta, z)$ and (f) $T(r, z)$.

Θ and in axial direction z, having both the same absolute value of 147 MPa (Tables 2 and 3), the same result as the one that would be obtained with Roark formulation for thin cylinders with radial temperature variation (Young and Budynas, 2002):

$$\sigma_\Theta = \sigma_z = \frac{\Delta T \alpha E}{2(1-\nu)} \tag{13}$$

5.2.2. Temperature field influence without radial variation

If temperature only varies circumferentially and axially T(Θ,z) as Fig. 13c, the tube bends under the action of the temperature variation in Θ coordinate. At $\Theta = 0°$ the tube has a greater temperature than at $\Theta = 180°$, thus the front face tries to expand more than the rear part of the tube and therefore the tube will tend to bend. Thermal stress increases as a consequence of clips, preventing the free motion of the tube.

In this case, it can be noticed in Fig. 13d that the stress distribution is similar to the original case. Equivalent stress values are slightly lower than in Fig. 10, where the temperature varies also radially (see Table 3). Without temperature gradient across the thickness, there are no internal constraints between inner and outer walls. If clips are not used the stresses decrease considerably

5.2.3. Temperature field influence without axial variation

It is important to note the difference that implies the presence of the axial temperature variation in the stresses. For this reason, it has been supposed that the temperature does not change in the axial direction and it remains constant ($T(r, \Theta)$), with respect to the temperature gradient in $z = 5.5$ m

the cross section (see Fig. 13e).

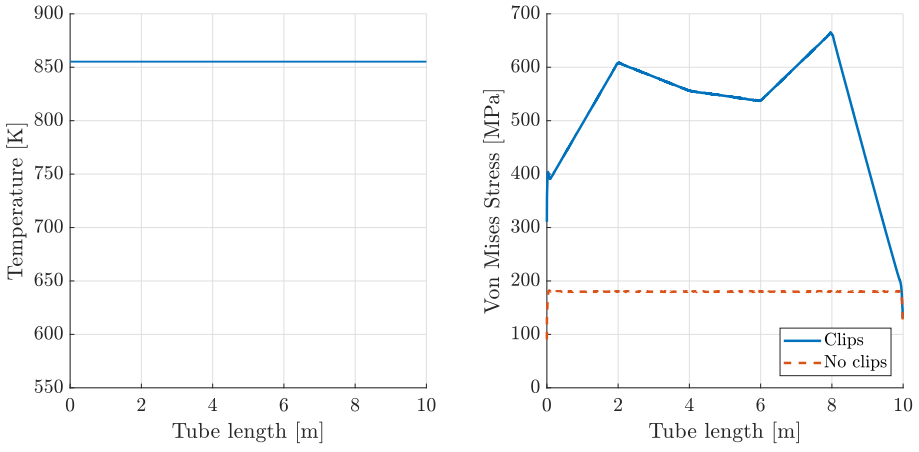

(a) (b)

Fig. 14: At $\Theta = 0°$, for $T(r, \Theta)$, (a) outer wall temperature and (b) Von Mises stress [MPa].

Fig. 14a depicts the temperature distribution along the tube length (constant for the current simplification), while Fig. 14b shows the equivalent stress with and without clips. When the deflection is not mechanically restricted, stress remains constant along the axial direction, with a value of 180 MPa (dashed line in Fig. 14b), the same as the maximum value of Fig. 11b dashed line. When mechanical restrictions are present (solid line in Fig. 14b), the stress distribution varies along the tube depending of the clips position.

The stress increases and the peak stresses are found in two different points (2 and 8 meters), compared with the original case (5.5m, Fig 11b). The deflection is greater because of the temperature gradient, in the tube cross section for $T(r, \Theta)$, is equal to the maximum reached in the original temperature distribution. Obviously, the reactions in the tube supports have changed, and the stress distribution along the axial direction is also differ-

ent. Assuming that the temperature does not vary axially, an overestimation of the stress due to the mechanical constraints is obtained. In fact, the maximum deflection without clips is larger than 7 m, the value with the real temperature field (Fig. 7a).

5.2.4. Summarizing the stresses for temperature distribution simplifications

Tables 2 and 3 summarises the maximum stresses depending on the temperature simplifications for cases without and with clips. In cases where the temperature distribution is not axisymmetric, the stress increases in the precense of clips.

The of Von Mises Stress for T(Θ,z) and T(r,Θ,z) differs less than 4%, because, in both cases stress, caused by the preventend thermal bending appears. For T(r,Θ) stresses are greater than in previos cases since the tube bending, that the clips avoid, is also greater, so the reaction forces increase.

	Without clips			
Stress component	T(r,Θ,z)	T(Θ,z)	T(r,z)	T(r,Θ)
σ_z [MPa]	224	211	147	223
σ_Θ [MPa]	97	41	147	97
σ_{VM} [MPa]	191	209.2	147	191

Table 2: Maximum absolute stress values without clips for every Temperature distribution analyzed.

	With clips				
Stress component	T(r,Θ,z)	T(Θ,z)	T(r,z)	T(r,Θ)	T(r,Θ)$_{Eqs.4,5,9}$
σ_z [MPa]	603	520	147	707	536
σ_Θ [MPa]	97	41	147	97	70
σ_{VM} [MPa]	560	539.5	147	665	505

Table 3: Maximum absolute stress values with clips for every Temperature distribution analyzed.

If only the tube maximum stress is needed, for example, in a fatigue analysis, the simplified temperature distribution $T(\Theta, z)$ gives a good aproximation of the stress value (see Table 3). The outer wall temperature has to be used in order to have the greater circumferential temperature variation. In addition, the 2D numerical approximation T(r,Θ) overestimates (20%) the equivalent stress, whereas the analytical approximation (Eqs. 6, 7, 11) underestimates (10%) such equivalent stress. This is because in the 2D numerical approximation the thermal stress is localized at tube clips whereas in the analytical approximation the thermal stress is uniformly distributed along the tube (infinite clips along tube length).

6. Conclusions

In this study, a finite element analysis of thin-walled tubes belonging to a molten salt receiver has been carried out. A finite element model has been developed in order to analyze the stress in the tube. The tube has been modelled mainly using shell elements; a tube slice has been modelled using solid elements in order to capture the full stress tensor.

The analysis of the tube cross section with solid elements, allows to determine that the most significant stress component is the axial stress, which has the highest absolute value followed by circumferential stress. The remaining stress components have a much lower magnitude and may be neglected, which reinforces the use of shell elements, because they consider these main stress components. These results are consistent with the existing literature.

Comparing stresses in the shell and solid parts reveals a difference around 4% between them, so tubes can be modelled with shell elements without a

significant error. Modelling tubes with shell elements allows to obtain thermoelastical stress distribution arised by the thermal and mechanical conditions in a 3D model.

In the present study it has been proved that clips (mechanical constraints) play an important role in the stress distribution of the receiver tubes. Results show that the stress component, that varies with the consideration of mechanical boundary conditions, is the axial stress. Therefore, tube thermal stress has two components: a component from the internal constraints, and another from the external constraints. This last constraint comes from the clips, which prevents thermal bending, increasing about three times the equivalent stress.

An analytical method proposed in the literature have been tested to check the validity to use them to calculate the thermal stresses. Results have shown that although, it does not consider axial temperature variation, this analytical aproach is an accurate approximation for calculating the maximum stress in the receiver tubes, obtaining just a slightly lower equivalent stress value respect to the finite element model.

The stresses obtained using simplified temperature distributions has been studied. Although radial temperature variation induces thermal stress due to the difference between inner and outer wall temperature, its influence is lower than the stress caused by the circumferential variation. The angular temperature distribution in the tube cross section produces a bending deformation, that should be prevented by mechanical restraints. Therefore, the thermal stress produced by the clips appear. Thermal bending is the main source of the equivalent stress, so radial temperature variation can be

neglected as first approximation.

Finally, the tube axial temperature is a key factor in the stress distribution along the tube receiver. If circumferential and radial variations are only taken into account, the stress distribution will be totally different from the corresponding to a axial variations with supports. Maximum stresses can be obtained accurately using 2D analytical aproximation. However, the assumption that the temperature does not varies axially avoids obtaining the correct temperature distribution along the tube. Note that in solar receiver tubes, where the aiming strategy modifies the temperature distribution axially, the stresses will also depend on the heliostats aiming.

Nomenclature

Roman symbols

A	tube cross section area (m^2)
a	tube inner radius (m)
B, D	Fourier coefficients
b	tube outer radius (m)
E	Young's modulus [Pa]
K	geometric thermal stress term [K]
r	tolar radial coordinate [m]
T	temperature [K]
$\overline{T}$	mean temperature [K]
ΔT	temperature difference between inner and outer surfaces of cylinder. [K]
z	coordinate in the axial direction [m]

Greek symbols

α	linear thermal expansion coefficient [K^{-1}]
ε	deformation
Δ	difference operator
ν	Poisson's ratio
Θ	polar angular coordinate [rad]
σ	stress [MPa]

Abbreviations

HTF	heat transfer fluid

Subscripts

i	inner surface
o	outer surface
Θ	circumferential component
r	radial component
z	axial component
VM	Von Mises

Acknowledgements

This work has been supported by the Iberdrola Fundation Spain under the fellowship "Ayudas a la investigacin en energía y medio ambiente". M.R. Rodríguez-Sánchez and D. Santana would like to thank the Ministerio de

Economía y Competitividad the support of the project ENE2015-69486-R (MINECO/FEDER, UE)

References

American Society of Mechanical Engineers, 2010. ASME Boiler and Pressure Vessel Code II, part D: Properties (Metric) Materials. Tech. rep., ASME, New York, USA.

Barron, R. F., Barron, B. R., 2011. Design for Thermal Stresses. Engineering case studies online. Wiley, New Jersey.

Boley, B. A., Weiner, J. H., 1997. Theory of Thermal Stresses. Dover Civil and Mechanical Engineering Series. Dover Publications.

Du, B. C., He, Y. L., Zheng, Z. J., Cheng, Z. D., 2016. Analysis of thermal stress and fatigue fracture for the solar tower molten salt receiver. Applied Thermal Engineering 99, 741–750.

Gatewood, B. E., 1941. Thermal stresses in long cylindrical bodies. The London, Edinburgh, and Dublin Philosophical Magazine and Journal of Science 32 (213), 282–301.

Goodier, J. N., 1937. Thermal stress in long cylindrical shells due to temperature variation roun the circumference and through the wall. Canadian Journal of Research 15a (4), 49–58.

Goodier, J. N., 1957. Thermal stresses and deformation. Journal of Applied Mechanics 24 (3), 467–474.

Hetnarski, R. B., Eslami, M. R., 2010. Thermal Stresses – Advanced Theory and Applications. Solid Mechanics and Its Applications. Springer Netherlands.

Irfan, M. A., Chapman, W., 2009. Thermal stresses in radiant tubes due to axial, circumferential and radial temperature distributions. Applied Thermal Engineering 29 (10), 1913–1920.

Kent, C. H., Ark, F., 1931. Thermal stress in thin-walled cylinders. Transactions of the American Society of Mechanical Engineers 53 (13), 167–180.

Litwin, R. Z., 2002. Receiver System : Lessons Learned from Solar Two Receiver System : Lessons Learned From Solar Two. Tech. Rep. SAND2002-0084, Sandia National Labs, Canoga Park.

Logie, W. R., Pye, J. D., Coventry, J., 2018. Thermoelastic stress in concentrating solar receiver tubes: A retrospect on stress analysis methodology, and comparison of salt and sodium. Solar Energy 160, 368–379.

Marugán-Cruz, C., Flores, O., Santana, D., García-Villalba, M., 2016. Heat transfer and thermal stresses in a circular tube with a non-uniform heat flux. International Journal of Heat and Mass Transfer 96, 256–266.

McDowell, M., Miner, K., 2013. Concentrating Solar Power Central Receiver Panel Component Fabrication and Testing. Tech. Rep. RD10-158, Pratt & Whitney Rocketdyne, Canoga Park.

Neises, T. W., Wagner, M. J., Gray, A. K., 2014. Structural Design Considerations for Tubular Power Tower Receivers Operating at 650 °C. Tech. Rep. April, NREL, Boston, Massachusetts.

Rodríguez-Sánchez, M. R., Soria-Verdugo, A., Almendros-Ibáñez, J. A., Acosta-Iborra, A., Santana, D., 2014. Thermal design guidelines of solar power towers. Applied Thermal Engineering 63 (1), 428–438.

Sánchez-González, A., Rodríguez-Sánchez, M. R., Santana, D., 2017. Aiming strategy model based on allowable flux densities for molten salt central receivers. Solar Energy 157, 1130–1144.

Sánchez-González, A., Santana, D., 2015. Solar flux distribution on central receivers: a projection method from analytic function. Renewable Energy 74, 576–587.

Sauer, G., 1996. Simple formulae for the approximate computation of axial stresses in pipes due to thermal stratification. International Journal of Pressure Vessels and Piping 69 (3), 213–223.

Timoshenko, S., Goodier, J. N., 1951. Theory of Elasticity, by S. Timoshenko and J.N. Goodier, 2nd Edition. Vol. 49. McGraw-Hill Book Company.

Uhlig, R., Frantz, C., Flesch, R., Fritsch, A., 2017. Stress Analysis of External Molten Salt Receiver. In: SolarPaces. Santiago de Chile, pp. 1–8.

Wagner, M. J., 2008. Simulation and Predictive Performance Modeling of Utility-Scale Central Receiver System Power Plants. Ph.D. thesis, University of Wisconsin-Madison.

Wang, F., Shuai, Y., Yuan, Y., Liu, B., 2012. Effects of material selection on the thermal stresses of tube receiver under concentrated solar irradiation. Materials & Design 33 (Supplement C), 284–291.

Young, W. C., Budynas, R. G., 2002. Roark's formulas for stress and strain, 7th Edition. McGraw-Hill.

Zavoico, A. B., 2001. Solar Power Tower: Design Basis Document. Tech. rep., Sandia National Laboratory, San Francisco, SAND2001-2100.